ACS OMEGA

Open Access

http://pubs.acs.org/journal/acsodf

Article

Selective Targeting of Lung Cancer Cells with Methylparaben-Tethered-Quinidine Cocrystals in 3D Spheroid Models

Sritharan Krishnamoorthi, Gokula Nathan Kasinathan, Ganesan Paramasivam, Subha Narayan Rath,* and Jai Prakash*

Cite This: *ACS Omega* 2023, 8, 46628−46639

Read Online

ACCESS | Metrics & More | Article Recommendations | Supporting Information

ABSTRACT: The development and design of pharmaceutical cocrystals for various biological applications has garnered significant interest. In this study, we have established methodologies for the growth of the methylparaben−quinidine cocrystal (MP−QU), which exhibits a well-defined order that favors structure−property correlation. To confirm the cocrystal formation, we subjected the cocrystals to various physicochemical analyses such as powder X-ray diffraction (PXRD), single-crystal X-ray diffraction (SCXRD), Raman, and IR spectroscopy. The results of the XRD pattern comparisons indicated no polymorphisms, and density functional theory (DFT) studies in both gaseous and liquid phases revealed enhanced stability. Our *in silico* docking studies demonstrated the cocrystal's high-affinity binding towards cancer-specific epidermal growth factor receptor (EGFR), Janus kinase (JAK), and other receptors. Furthermore, *in vitro* testing against three-dimensional (3D) spheroids of lung cancer (A549) and normal fibroblast cells (L929) demonstrated the cocrystal's higher anticancer potential, supported by cell viability measurements and live/dead assays. Interestingly, the cocrystal showed selectivity between cancerous and normal 3D spheroids. We found that the MP−QU cocrystal inhibited migration and invadopodia formation of cancer spheroids in a favorable 3D microenvironment.

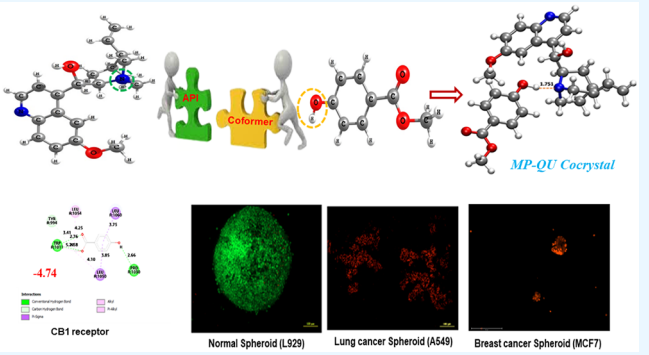

INTRODUCTION

Crystal engineering has emerged as a reliable method for producing novel crystalline lattices with improved characteristics. A cocrystal, which consists of a well-defined stoichiometry of two or more different chemical entities through non-covalent interactions, is an example of a structurally homogeneous crystalline complex. These cocrystals exhibit distinct physicochemical properties compared to the individual components.[1,2] In recent decades, this area of research has seen a remarkable increase in potential applications, including gas storage in porous solids, synthetic ferroelectrics at ambient temperature, non-linear optical (NLO) active materials, and sensors.[3−5]

Crystal engineering based on active pharmaceutical ingredients (APIs) has gained significant attention due to its well-defined crystalline nature. Approximately 40% of commercially available compounds and 70% of drug molecules under development face challenges related to solubility and other crucial parameters.[6] As a result, pharmaceutical cocrystals that incorporate APIs and undergo varied solid-phase changes have been developed to improve physicochemical properties such as thermal stability, mechanical properties, dissolution rate, solubility, hygroscopicity, tablet ability, flowability, and bioavailability of drugs.[7−9] Researchers have made significant efforts to investigate crystal and supramolecular structures, solubility, melting point, and other characteristics.[10−13] For example, Saha *et al.* cocrystallized quinoxaline, a commonly used API for multiple anticancer drugs, with 3-thiosemicarbano-butan-2-one-oxime, which elevated the anticancer activity against lung cancer cells.[14] Cocrystallization of betulinic acid and ascorbic acid has also shown immense antiproliferative activity.[15] Furthermore, cocrystallization of 5-fluorouracil, a drug already in use for cancer treatment, with nicotinamide has improved the overall efficacy.[16] Various cocrystallization strategies have been employed with both existing drug molecules and completely new combinations of molecules to enhance biopharmaceutical values.[15−19]

Malignant neoplasms, or cancer, are characterized by uncontrolled cell growth. Despite advancements in the field of oncology, cancer remains a leading cause of death worldwide, identified by the World Health Organization

Received: August 1, 2023
Revised: October 25, 2023
Accepted: November 2, 2023
Published: November 21, 2023

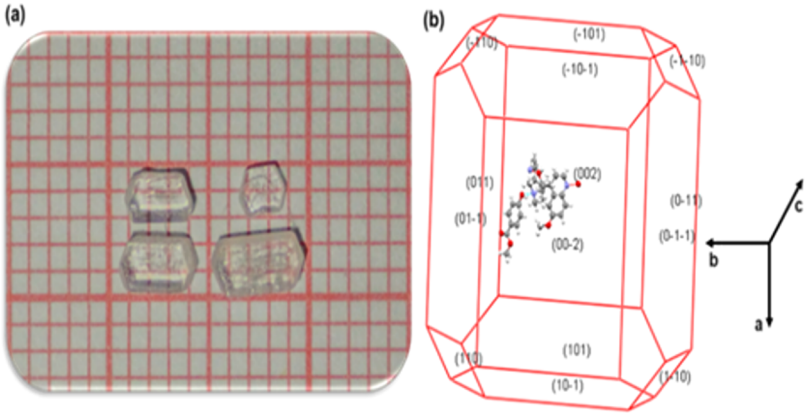

Figure 1. Photograph of (a) MP−QU cocrystals and (b) BFDH morphology diagram of the MP−QU cocrystal.

(WHO) as the second major cause of death.[20] Millions of people in developed and developing countries are affected. However, drugs that target cancer cells are still inefficient and often result in serious side effects on rapidly regenerating normal tissues. Therefore, there is a crucial need to develop a methodology to obtain drugs with optimal selectivity toward solid tumors.

Drug development is a complicated and challenging process. Most drugs that have shown efficacy in two-dimensional (2D) adherent cell culture models often fail during clinical trials.[20] The problem with adherent monolayer cultures is that they lack the complexity and dynamics of native malignant tissues.[21] Cell-to-cell junctions are only at the periphery, and there is no interaction with the extracellular matrix (ECM), which can alter gene expression. To overcome these limitations, three-dimensional (3D) spheroids are highly recommended for testing drugs or any molecule.[22,23] Spheroids can mimic the tissue-like framework of native malignant tissues, including the ingress and egress of nutrition, hypoxia, drug penetration and resistance, inter- and intracellular signaling, and heterogeneity within the tumor region, including the deposition of ECM. Spheroids have three different regions similar to a solid tumor: (1) a central necrotic core, (2) a middle quiescent region, and (3) a peripheral proliferative region. The peripheral proliferative regions of a tumor are characterized by ample diffusion of nutrients and exchange of by-products, while the central core region is deficient in diffusion, leading to a necrotic core. The middle quiescent region of the spheroid is highly significant because it facilitates signal transduction between the regions, and constantly signals for overcoming drug actions and adapting a pathway for better tumor survival. Spheroids are an excellent tool for modeling solid tumors, as they not only replicate the physical features of the tumor but also mimic the chemistry of the tumor micro-environment, including the expression profile and pro-survival signaling pathways that contribute to tumor progression. This makes spheroids a valuable tool for studying and testing new treatments for cancer.[23] Testing drugs on spheroids that successfully overcome the growth and proliferation of 3D cancer models can be considered as potential candidates for further development phases.

To our knowledge, there have been no studies on cocrystals with potential anticancer properties tested on 3D lung cancer models. In this current investigation, we utilized an innovative approach to grow pharmaceutical methylparaben−quinidine cocrystal (MP−QU) cocrystals using three different methods. The grown cocrystals were subjected to various analytical techniques for characterization purposes. We also examined the specific cytotoxicity of the quinidine-based cocrystal on 3D lung cancer models and investigated its structural properties. In addition, *in silico* structural studies were conducted, which showed the cocrystal's potential antibacterial, antimalarial, and specific anticancer targeting properties through docking analysis. Furthermore, the cocrystal's sustained stability was verified through density functional theory (DFT) analysis.

EXPERIMENTAL METHODS

Cocrystallization of MP−QU. To perform the slow evaporation method, we started by dissolving an equimolar mixture of MP (152.15 mg, 1 mmol) and QU (324.4 mg, 1 mmol) in acetone (45 mL) to obtain a transparent, white solution. The solution was then carefully sealed to prevent any dust or solvent evaporation. After allowing the solution to sit undisturbed for 2 days, we observed the formation of colorless, prism-like crystals. We carefully harvested these crystals for further analysis.

In the rotary evaporation method, an equimolar mixture of MP (152.15 mg, 1 mmol) and QU (324.4 mg, 1 mmol) was dissolved in 45 mL of acetone as a solvent. The solution was then subjected to vacuum rotary evaporation at 49 °C, which resulted in the formation of colorless crystals. The obtained MP−QU cocrystals were then dried in a vacuum oven at 27 °C for 15 h.

To prepare the MP−QU cocrystals using the solvent-drop grinding method, we first mixed MP (152.15 mg, 1 mmol) and QU (324.4 mg, 1 mmol) in a stoichiometric ratio of 1:1 using an agate mortar and pestle. The resulting mixture was then ground for 10 min before slowly adding small amounts of acetone drop by drop. The mixture was then further ground for about 20 min, after which the MP−QU cocrystals were obtained.

RESULTS AND DISCUSSION

Crystal Growth of the MP−QU Cocrystal. The polymorphic behavior of MP−QU cocrystal was investigated using three versatile crystallization methods, namely, slow evaporation, rotary evaporation, and solvent-drop grinding crystallization with acetone as the solvent. Among the three methods, the solvent-drop grinding method was found to be the most effective for the synthesis of the cocrystal and was therefore utilized as the primary method.[24] Polymorphism in cocrystals is of great interest because crystal engineering of

https://doi.org/10.1021/acsomega.3c05617
ACS Omega 2023, 8, 46628−46639

pharmaceutical cocrystals can help fine-tune certain properties. Although we tried different crystallization methods for growing MP−QU cocrystals, no polymorphic changes were observed. The structure of the MP−QU cocrystal was found to be in the ratio 1:1, which was confirmed by single-crystal X-ray diffraction (SCXRD) analysis. The crystal structure and photograph of the grown MP−QU cocrystal are shown in Figure 1a. The theoretical Bravais, Friedel, Domnnay, and Harker (BFDH)[25] morphology structure of the cocrystal was determined with the MERCURY software using the unit cell parameters of the grown cocrystal and is shown in Figure 1b.

XRD Analysis and DFT Study for the MP−QU Cocrystal. The utilization of MP and QU materials enhances the ability of the method to form a multicomponent molecular complex. Pharmaceutical cocrystals synthesized using these materials are commonly applied in crystal engineering principles, thanks to the electrostatic interaction between the hydroxyl and N atoms of heterosynthon. Quinidine, consisting of a quinoline aromatic ring, a quinuclidine ring (a tertiary amine), and a methylene alcohol group binding them together, provides the necessary molecular structure for cocrystal formation.[26] The ester carbonyl group ($-COOCH_3$) and hydroxyl group (−OH) of methylparaben act as electron acceptors and donors, respectively, due to the intermolecular electron transfer that occurs.[27] Theoretical elucidation of cocrystal formation can be done using DFT studies, with the optimized molecular geometric structure in the gas phase presented in Figure 2. The MP interacts with QU at a 3-

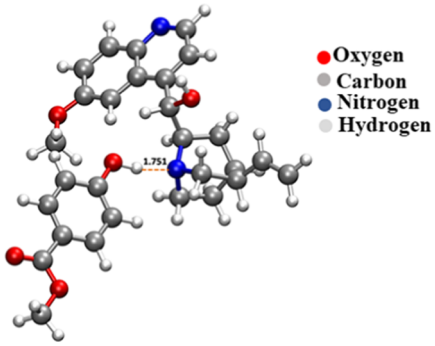

Figure 2. Optimized structure of a MP−QU cocrystal in gas phase. The O−H···N intermolecular interaction is shown as a dotted line with a bond length in Å.

coordinated N atom through a weak O−H···N bond with a bond length of 1.75 Å. Due to the negativity of the N atom with a Mulliken charge of −0.075*e*, the formation of the cocrystal is initiated by attracting the proton H of methylparaben, which is further stabilized by multiple weak hydrogen bonds ranging from 2.46 to 3.31 Å. The relaxation of the structure in the solvent phase (Figure S1) shows further strengthening of the O−H···N bond length by contracting 0.05 Å in both acetone and ethanol solvents, implying that the solvent medium facilitates the stabilization of the cocrystal. The calculated highest occupied molecular orbital−least unoccupied molecular orbital (HOMO−LUMO) gap is 4.50 eV in the gas phase and increases slightly by 0.0004 eV, confirming the stability of the cocrystal even under solvent conditions. To understand the structural changes leading to variation in the interaction between MP and QU in different phases such as gas, liquid, and solid, the bond angle was measured between MP and QU. The bond angle O−H···N between MP and QU is 166.774° in the gas phase, 167.496° for ethanol, and 167.477° for acetone. In crystal form, the bond angle is 155.594°, implying that there is a molecular rotation of MP in different phases, leading to a reduction of 11.180° in crystal form, which in turn results in a strong interaction between MP−QU in the obtained cocrystal.

The stability of the pharmaceutical MP−QU cocrystal is governed by both inter- and intramolecular hydrogen bonding, as evidenced by theoretical studies. The experimental PXRD pattern of the cocrystal was ascertained by comparing it to the simulated pattern obtained from SCXRD (Figure S2). The cocrystal was successfully grown in acetone as the solvent using an equivalent molar ratio of MP and QU (1:1). The resulting cocrystal structure is orthorhombic with a non-centrosymmetric space group $P2_12_12_1$, $Z = 4$, and unit cell parameters of $a = 9.9190$ (3) Å, $b = 11.8192$ (4) Å, and $c = 21.6689$ (7) Å.[19] The unit cell comprises four MP and four QU molecules. Crystallographic structural information parameters for the MP−QU cocrystal are summarized in Table S1, while Table S2 provides the atomic coordinates of hydrogen and non-hydrogen atoms in the unit cell along with their corresponding isotropic atomic displacement parameters.

The Mulliken charge analysis revealed that the nitrogen atom of QU has a more negative charge of −0.075*e*, while the oxygen and hydrogen atoms of MP have charges of −0.274 and 0.461*e*, respectively. This suggests that the formation of the MP−QU cocrystal is driven by the interaction between the positively charged proton (H) and negatively charged anion (N). The natural bond orbital (NBO) analysis showed that the natural atomic charges for N, O, and H are −0.57, −0.73, and 0.51*e*, respectively, which is in good agreement with the Mulliken charges. Moreover, the natural charges slightly increase upon introduction of the solvent. All calculated partial charges of the MP−QU cocrystal are listed in Table S3. The elongation of the O−H bond length by ∼0.011 Å in the solvent environment can be attributed to the decrease in the natural charge of an oxygen atom and the increased charge of the hydrogen atom. Similarly, the weak N···H−O interaction is strengthened by the increase in the natural charges of N and O atoms in the presence of a solvent. The solvent environment, therefore, enhances the stability of the MP−QU cocrystal instead of destabilizing it.

Atoms in Molecule (AIM) Analysis. To investigate the nature of the interaction between MP and QU molecules in the cocrystal, an analysis of the N···H−O bond was conducted using the relaxed geometry at the B3LYP/6-311++G** level with atoms in molecules (AIM) analysis.[28−30] The bond critical point (BCP) or saddle point of a chemical bond, which represents the point at which the electron density is low between two interacting atoms in a molecule, was characterized in the AIM analysis. BCP properties, such as ρ and its derivatives, $\nabla^2\rho$, were calculated to accurately describe the electronic structure of the molecular system. The BCP properties are summarized in Table S4. The electron density (ρb) at a BCP is associated with the strength of an atomic interaction corresponding to a chemical bond. For the N···H−O interaction in the MP−QU cocrystal, the electron density ρ obtained was 0.0510 au. This value is lower than that of conventional covalent bonds (C−C, $\rho = 0.241$ au) but higher than that of neutral hydrogen bonds.[31]

The formation of the MP−QU cocrystal is primarily governed by the N···H−O interaction, which is characterized using the Laplacian of electron density ($\nabla^2\rho$ (N···H−O)) at

https://doi.org/10.1021/acsomega.3c05617
ACS Omega 2023, 8, 46628−46639

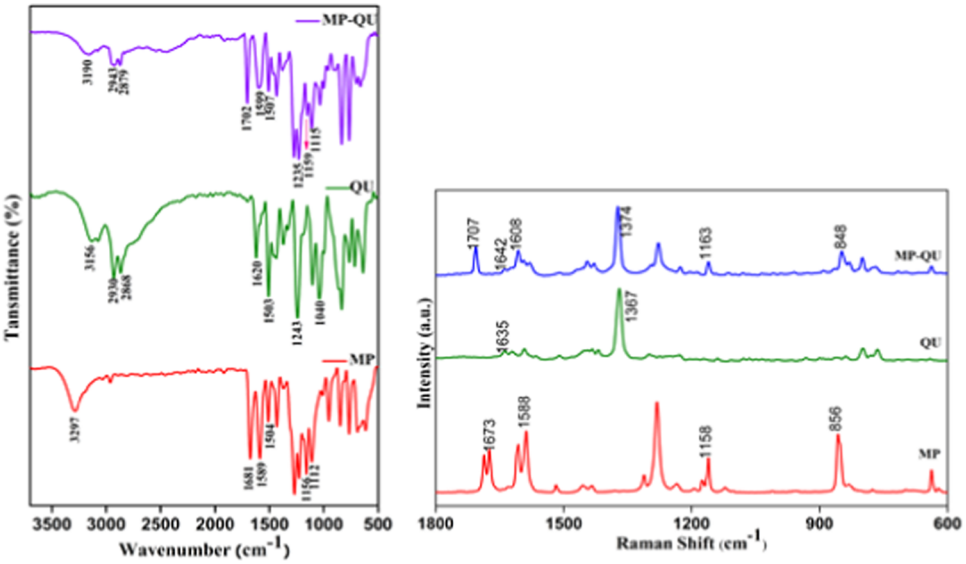

Figure 3. (Left) FT-IR and (right) Raman spectra of MP−QU cocrystals in comparison with their starting materials.

the bond critical point (BCP). The positive value of Laplacian ($\nabla^2\rho > 0$) given in Table S5 signifies the dominant electrostatic nature of the interaction. However, the negative value of total energy $H(r)$ suggests that the bonding interaction is stabilized by the accumulation of electrons at the BCP, indicating a covalent character. Thus, the N···H−O interaction is crucial for the formation of the MP−QU cocrystal.

Spectroscopic Analysis of Cocrystals. The functional groups present in the molecular structure were analyzed using spectroscopic techniques, such as Fourier transform infrared (FT-IR) and Raman spectroscopy. The formation of the cocrystal was evidenced by the resultant spectra of pure MP, QU, and the MP−QU cocrystal (Figure 3). In the pure MP spectrum, the peaks corresponding to ester C═O stretching were observed at 1681 cm^{-1}. The C−O−C symmetric and asymmetric stretching modes of vibrations were observed at 1156 and 1112 cm^{-1}, respectively.[27] Similarly, the spectrum of pure QU displayed peaks corresponding to O−H stretching, C−O stretching, and C═N stretching modes at 3156, 1243, and 1503 cm^{-1}. The MP−QU cocrystal exerted a significant change in the above-discussed vibrational modes of the pure forms of MP and QU. The MP−QU spectra displayed shifts in the ester C═O and νC−O−C to 1702, 1159, and 1115 cm^{-1}, respectively, from their pure forms (MP and QU) individually. Other shifts witnessed included O−H, C═N, and C−O stretching frequencies of 3190, 1507, and 1235 cm^{-1}, respectively. This supports the presence of intermolecular interactions in the grown MP−QU cocrystal. Further, the FT-IR study confirmed the participation of the hydroxyl group of the coformer and the amine group of quinidine in the formation of hydrogen bonding. These observations indicate that the amine and hydroxyl groups strongly participate in the formation of hydrogen bonding in the grown MP−QU cocrystals.

The Raman spectra of MP and QU were analyzed to investigate the intermolecular interactions in the grown cocrystal. In the Raman spectra of pure MP, C═O stretching modes were observed at 1588 and 1673 cm^{-1}. However, for the cocrystal, these values were shifted to 1608 and 1707 cm^{-1}, respectively. The COO stretching vibration frequency appeared as an intense sharp peak at 1282 cm^{-1} for pure MP and it was shifted to 1276 cm^{-1} in the cocrystal. In the Raman spectra of pure QU, the C═N stretching frequency appeared at 1635 cm^{-1} and C−O stretching modes were observed at 1367 cm^{-1}. Upon formation of the cocrystal, these frequencies were shifted to 1642 and 1374 cm^{-1}, respectively. The significant shifts in these vibrational modes provide evidence for the formation of intermolecular interactions in the grown MP−QU cocrystal.

Differential Scanning Calorimetry. The physicochemical and pharmacokinetic properties of APIs, coformers, and cocrystals are influenced by their thermal stability and phase transitions. To investigate the thermal behavior of the MP−QU cocrystal, DSC experiments were performed (Figure 4).

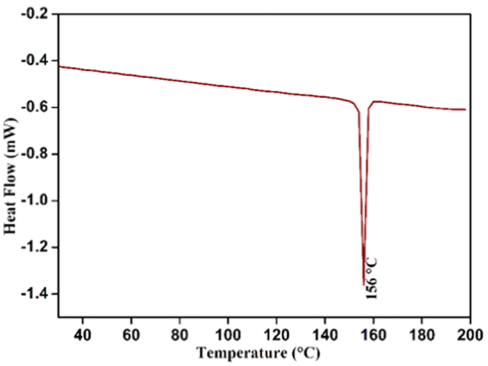

Figure 4. DSC thermogram of the grown MP−QU cocrystal.

Literature reports indicate that the MP crystal exhibits a sharp endothermic peak at 127 °C,[27] while the QU crystal shows a sharp endothermic peak at 175 °C.[19] However, the cocrystal exhibited a sharp endothermic peak at 156 °C. This suggests that the value of cocrystal lies between that of the API and the coformer, indicating that their interaction induces the formation of a new phase. These findings were in good agreement with the X-ray and spectroscopic analyses. Moreover, the cocrystal exhibited good thermal stability between 30 and 150 °C, with no phase transmission observed. This

https://doi.org/10.1021/acsomega.3c05617
ACS Omega 2023, 8, 46628−46639

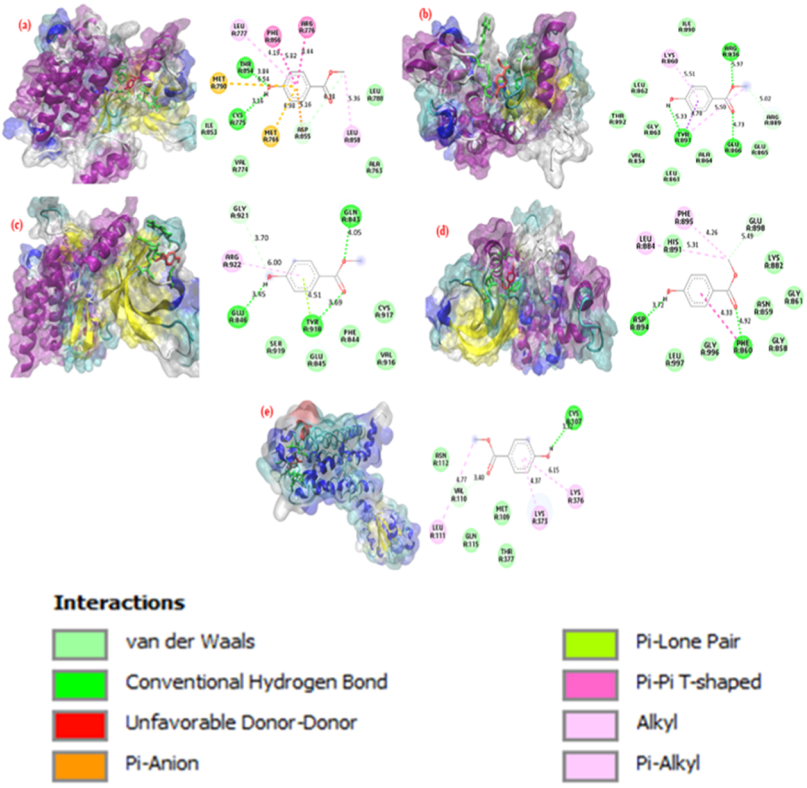

Figure 5. Binding interaction of MP−QU with (a) 5D41, (b) 2ITO, (c) 4F09, (d) 3FUP, and (e) 5XRA protein.

suggests that the cocrystals can be employed for various optical applications within this temperature range.

Molecular Docking Studies. Molecular docking studies were conducted using the Auto Dock 4.0 tool to evaluate the binding affinity of the MP−QU cocrystal with various protein targets known for their physiological functions in cell proliferation, signal transduction, and their potential as antimalarial, antibacterial, and anticancer agents. The docked poses were analyzed, visualized, and imaged in 2D and 3D using PyMol and Biovia Discovery Studio software.[31,32] All of the rotatable bonds inside the ligand were allowed to freely move, and the receptor was considered rigid. The antimicrobial protein targets [PDB ID: 1JZQ, 1KZN, 1UAG, 2VDI, 2VEG, 2ZDQ, 3RAE, 3SRU, 3TTZ, 3TYE], antimalarial protein targets [PDB ID: 2B1C, 1DLG, 1LS5, 2BL9, 1SME3, 3NTZ, 3QS1, 4DP3, 4DPD, 4W11, 4YDQ, 51FU, 5VAD], and anticancer proteins targets [PDB ID: 2RH1, 3NYA, 3POG, 3QAK, 4K5Y, 5NX2, 5XRA, 4OR2, 4QIN, 5C1M, 5EE7, 5UZ7, 2KI9] were downloaded from protein data bank (PDB) https://www.rcsb.org/. In addition to that, docking was performed for the epidermal growth factor receptor (EGFR) kinase receptor [PDB ID: 2ITO, 2ITY, 5D41, 5UGB, 6DUK, 2J6M, 1M17, 2ITW, 5CZI], Janus kinase (JAK) protein tyrosine kinase receptor [PDB ID: 3EYG, 3FUP, 3KRR, 4F08, 4F09], and JAK kinase protein 1s and 3 [5KHW, 7C3N, 7APG]. The binding free energy for the protein−cocrystal complex is determined. When the synthesized MP−QU cocrystal ligand was docked with EGFR kinase receptors, it showed the lowest binding energy value of −4.65 kcal/mol for 5D41 and −4.58 kcal/mol for 2ITO. The docked ligand interacted with nine amino acid residues of 5D41, namely, pi−pi interaction between ARG-776, PHE-856 and ligand with bond lengths of 8.44 and 5.82 Å, respectively, pi−alkyl interaction between LEU-858, LEU-777 and ligand with bond lengths of 5.36 and 4.19 Å, respectively, pi−lone pair interaction between MET-766, MET-790 and ligand with bond lengths of 4.98 and 6.54 Å, respectively, and hydrogen bonding interaction between THR-854, CYS-775 and ligand with bond lengths of 3.84 and 3.16 Å. The docked ligand interacted with four amino acid residues of 2ITO, namely, the hydrogen bond interaction between ARG-836, GLU-866, TYR-891 and ligand with bond lengths of 5.97, 4.73, and 4.70 Å respectively, pi−alkyl interaction between LYS-860, TYR-891 and ligand with bond lengths of 5.50 and 5.51 Å respectively, and pi−pi interaction between TYR-891 and ligand with a bond length of 4.70 Å. When the synthesized MP−QU cocrystal ligand was docked with the JAK protein tyrosine kinase receptor, it showed the lowest binding energy value of −4.66 kcal/mol for 4F09 and −4.63 kcal/mol for 3FUP. The docked ligand interacted with four amino acid residues of 4F09, namely, hydrogen bond interaction between GLN-843, TYR-918, GLU-846 and ligand with bond lengths of 4.05, 3.69, and 3.45 Å, respectively, pi−alkyl interaction between ARG-922 and ligand with a bond length of 6.00 Å, and pi−lone pair interaction between TYR-918 and ligand with 4.51 Å, respectively. The docked ligand interacted with four amino acid residues of 7C3N with the lowest binding free energy of −4.74 kcal/mol. Among four amino acids, GLU 1041 and ARG 1042 interact through hydrogen bonds with bond lengths of 4.59 and 5.92 Å, respectively. Additionally, Arg 1049 interacts through alkyl interaction with a bond length of 4.88 Å and ALA 1046 interacts through van der Waals interaction with a bond length of 5.95 Å.

The docked ligand interacted with six amino acid residues of 3FUP, that include, hydrogen bond at ASP-894, PHE-860 (bond lengths: 3.72 and 4.92 Å), pi−pi interaction at PHE-860

https://doi.org/10.1021/acsomega.3c05617
ACS Omega 2023, 8, 46628−46639

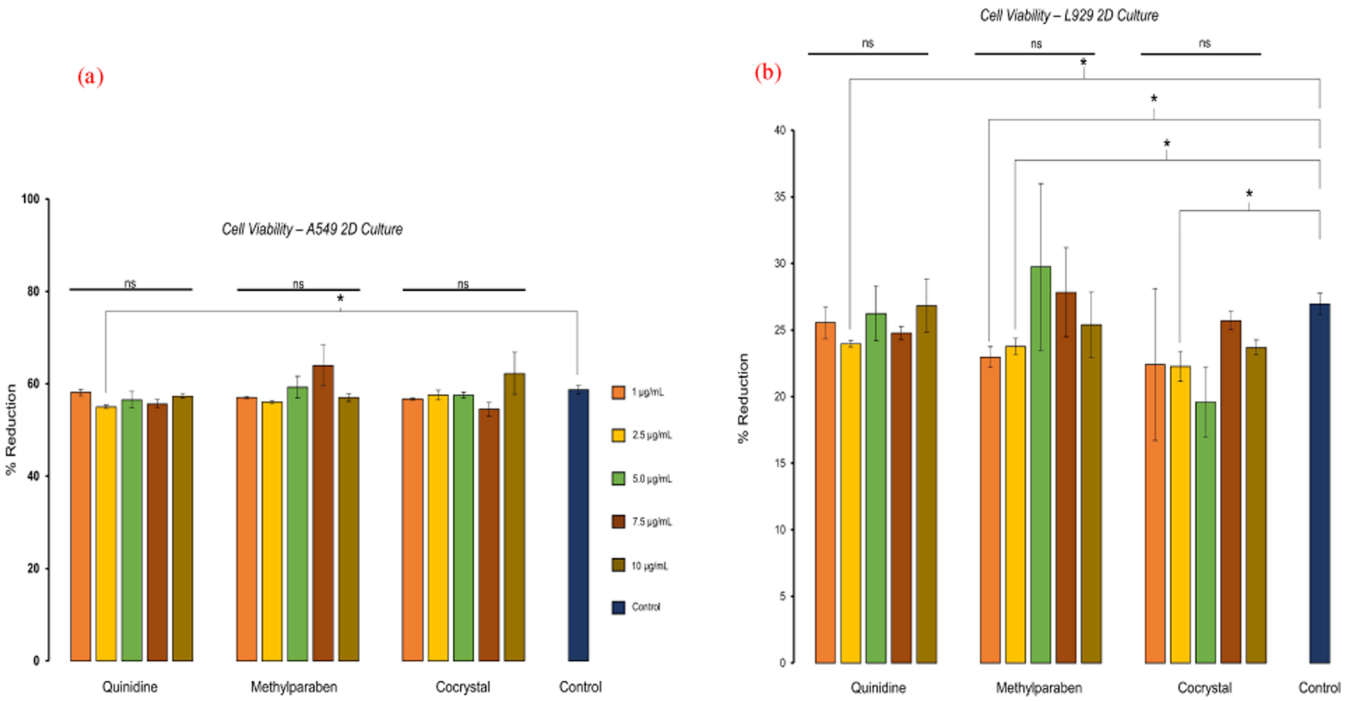

Figure 6. Cell viability on adherent format upon the MP−QU cocrystal treatments for 48 h. (a) A549 lung cancer cells and (b) L929 normal connective tissue/fibroblast cells (*indicates p-value < 0.05 and ** indicates p-value < 0.01).

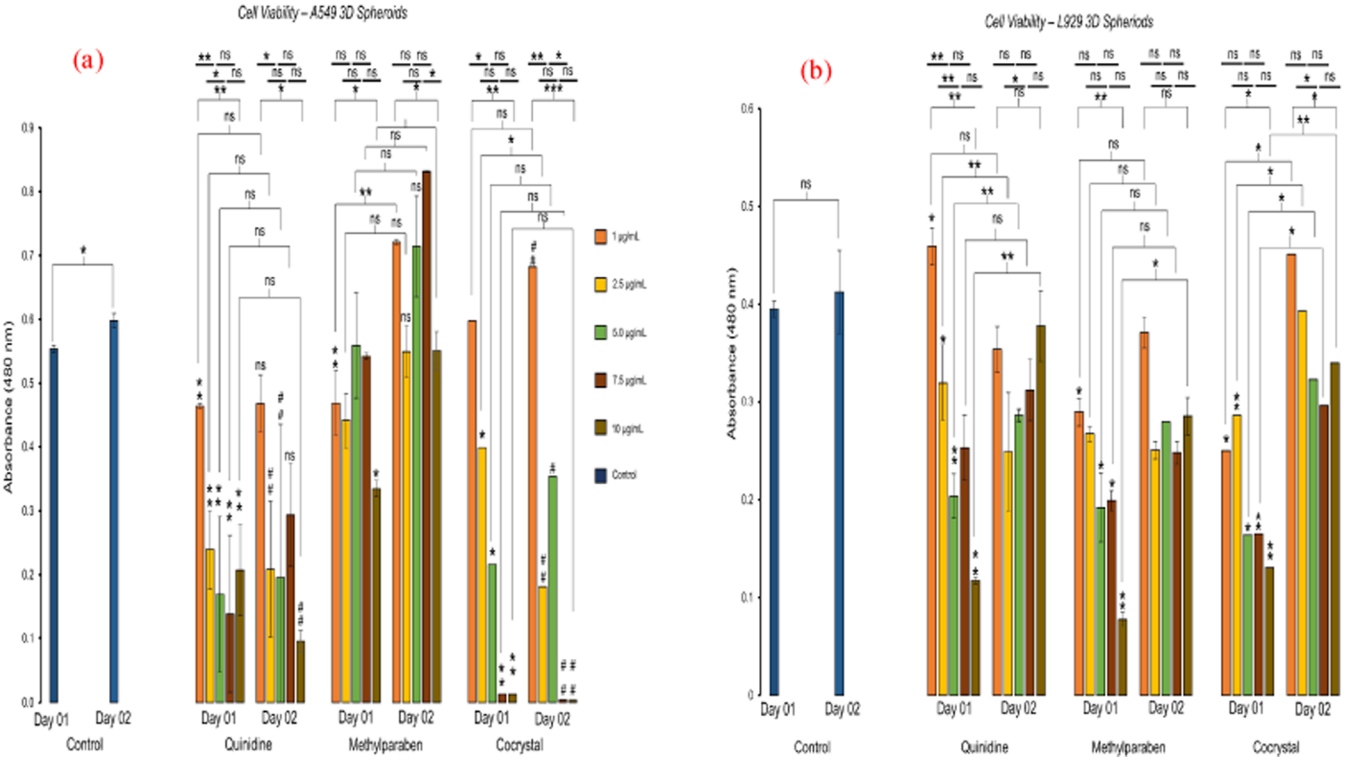

Figure 7. Cell viability of 3D spheroids upon MP−QU cocrystal treatments on day 01 and day 02. (a) A549 lung cancer cell spheroid and (b) L929 normal connective tissue/fibroblast cell spheroids (* indicates p-value < 0.05 and ** indicates p-value < 0.01).

(4.33 Å), alkyl interaction at LEU-884, PHE-895 (5.31 and 4.26 Å), and Van der Waals interaction at HIS-891 (5.31 Å) (Figure 5). Apart from these protein targets, the ligand shown interactions with antimicrobial targets 2VDI and 3SRU at VAL 69 and LEU 21, LEU 25, with the lowest binding free energy of −3.38 kcal/mol. Subsequently, the antimalarial targets found to be 1DLG and 1LS5 interact with ASN 197, ASP 143, and ASN 228, respectively, with a binding free energy of −4.34 kcal/mol and anticancer targets 5XRA interacts with Leu 111 with a binding free energy of −4.57 kcal/mol that is shown in Figure S3. *In silico* docking studies affirm that the cocrystal

https://doi.org/10.1021/acsomega.3c05617
ACS Omega 2023, 8, 46628−46639

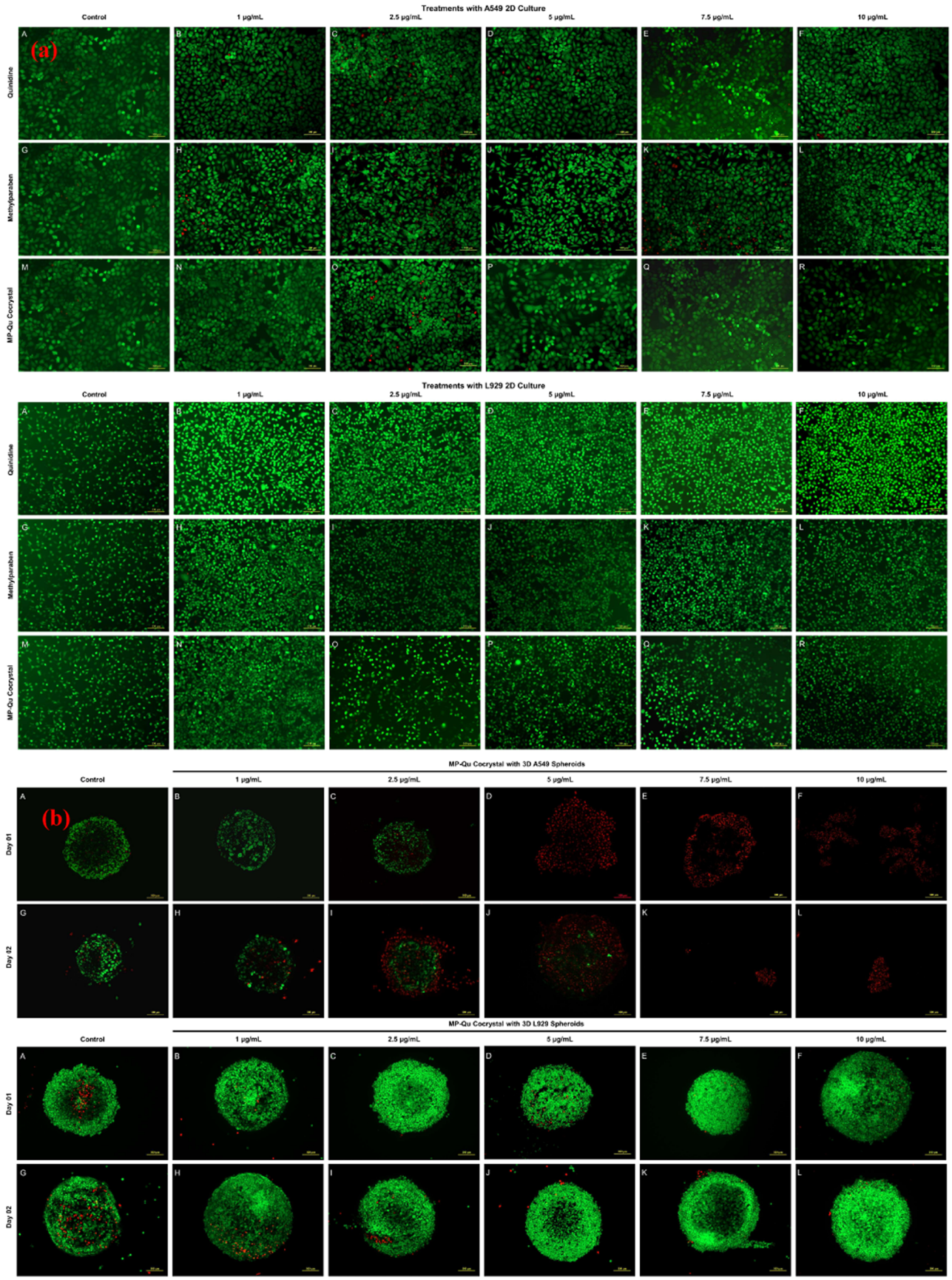

Figure 8. Live/dead staining of 2D adherent cells and 3D spheroids: Treatments with the MP−QU cocrystal with A549 cells and L929 in 2D adherent and 3D spheroids.

https://doi.org/10.1021/acsomega.3c05617
ACS Omega 2023, 8, 46628−46639

molecule binds with a good affinity toward antimicrobial, antimalarial, and anticancer protein targets.

***In Vitro* Studies.** Molecular studies have shown that quinidine (API) has potential impact on mammalian cells, as demonstrated in previous reports.[33−35] In this study, we investigated the anticancer activity of the cocrystal on highly metastatic lung adenocarcinoma cell line A549, as well as on a control cell line L929, which is a normal connective tissue cell line.

Treatments were performed on both 2D adherent cultures and 3D spheroids of A549 and L929 cells. Figure 6 illustrates the effect of quinidine cocrystal, quinidine, and coformer on A549 cells after 48 h of treatment. In 2D adherent cultures, the cocrystal or coformer did not significantly affect A549 cancer cells, while quinidine at a concentration of 25 μg/mL caused a significant decrease in cell viability compared to the control. For L929 cells, the cocrystal exhibited a noticeable decrease in cell viability at lower concentrations (2.5 μg/mL), while no other concentrations showed any impact on cell growth. Quinidine displayed similar activity at a concentration of 2.5 μg/mL, whereas MP only prevented cell growth at concentrations of 1 and 2.5 μg/mL.

Studies in the 3D Lung Cancer Model. Although the cocrystal did not show significant effects on the 2D cultures of the A549 cell line, we investigated its potential anticancer activity using 3D lung cancer spheroids, as quinidine has been reported to be more selective toward tumor cells and their metabolism (Figure 7).[34,36−38] Both L929 and A549 lung cancer spheroids were treated with the cocrystal and quinidine, and their viability was assessed on day 01 and day 02 of treatment. On day 01, the cocrystal and quinidine exhibited a similar pattern in preventing the growth of A549 spheroids, with the viability of A549 spheroids decreasing with increasing concentrations of both the cocrystal and quinidine, as compared to the control A549 spheroids.

To emphasize, the anticancer activity of the cocrystal was found to be significant at concentrations of 7.5 and 10 μg/mL, leading to a complete cessation of A549 lung cancer cell spheroid growth on day 02. This was in contrast to the control group and other cocrystal groups, indicating a potent effect of the cocrystal. Although quinidine showed appreciable activity on day 01, there was no significant change in spheroid viability on day 02. In contrast, methylparaben did not show any effect on day 01 but led to an increase in spheroid viability on day 02, indicating a reversal of effect. Although L929 spheroids showed some resistance to the treatments on day 01, their viability relapsed on day 02, following a pattern similar to those of quinidine and methylparaben. These results suggest the killing ability and selectivity of the cocrystal, likely due to the presence of the quinidine moiety.[36−38]

Live/Dead Assay. To confirm the selective anticancer properties of the synthesized cocrystal, 2D and 3D spheroids were examined using a live−dead staining assay under a fluorescence microscope (Figure 8a,b).

In the 2D adherent cell treatment (Figure 8a), the live/dead staining assay was consistent with the cell viability as no dead cells were observed for any concentration of A549 or L929 cells. Although L929 cells showed a decrease in cell viability with cocrystal treatment (2.5 μg/mL) in 2D, the cells were not visibly stained for PI. However, in the case of 3D spheroids on day 01 (Figure 8b), A549 spheroids treated with 7.5 and 10 μg/mL concentrations were completely dead, with very few live cells. Other concentrations of cocrystal (1, 2.5, 5.0 μg/mL) showed a mix of live and dead cells within the spheroids. The anticancer effect of the cocrystal at 7.5 and 10 μg/mL was consistent, as the spheroids were dead on day 01, with no live cells visible in any part of the spheroids even on day 02. The fluorescence assay complements the findings of cell viability and confirms the resistance of cancer cells in 3D spheroids. It is widely known that 3D spheroids mimic the actual cancerous tissue *in vivo*,[22,23] and our study found a contrast between drugs tested in 2D and 3D spheroids, emphasizing that 2D models are not always a reliable predictive tool for clinical trials.[39]

Despite the partial effect observed with other concentrations, the spheroids exhibited a similar number of live cells on day 02. In contrast, L929 spheroids showed a significant number of live cells on day 01 after treatment with cocrystals and only a few dead cells at the periphery. All cocrystal concentrations showed similar effects on L929 spheroids on day 01. Surprisingly, on day 02, L929 spheroids had even fewer PI-stained dead cells, indicating an increase in viability. To determine whether the anticancer activity was due to MP or quinidine, we tested each individually with 3D A549 spheroids at various treatment concentrations for 48 h. Live/dead assays were conducted on the treated spheroids, which showed that both MP and quinidine had no significant antiproliferative properties with A549 spheroids, as the treated spheroids were viable similar to control spheroids. Multiple fluorescence images were quantified for the number of green and red fluorescent stains using ImageJ software, and there was no significant difference between the percentage of live and dead cells (Figure S5, graph) with control spheroids and treated ones. MP has previously been shown to contribute to the progression and proliferation of breast cancer,[40,41] while the cocrystal combination of quinidine and MP showed anticancer properties. The selectivity of the cocrystal may be attributed to the presence of quinidine, which has specific targets such as Cannabinoid receptor 1 (CB1), Glucocorticoid receptor, MYC protein, etc., rather than relying on the hyperproliferative capacities of tumor cells over normal cells like traditional drugs.[34,36−38] L929 cells are highly metabolic and show fast growth without any harmful effects from the cocrystal after day 01. Quinidine's ability to selectively target normal cells has been reported previously and is likely responsible for the cocrystal's selectivity.[34,36,37,42]

To support the anticancer properties of the synthesized cocrystal, *in silico* docking studies were conducted and revealed the binding of the cocrystal with Cannabinoid receptor 1 (CB1, 5XRA) at a significant affinity. Recent reports have claimed that CB1/CB2 receptors are overexpressed in liver and breast cancers compared to normal cells.[37] Interestingly, our cocrystal carrying quinidine was predicted to have a high affinity in binding to the CB1 receptor, and quinidine has an inhibitory role with the CB1 receptor. Reports suggest that overexpression of CB1 and CB2 in cancer is due to progression and metastasis in nonsmall cell lung cancer (NSCLC).[43] The highly metastatic nonsmall cell lung carcinoma cell line A549 was used to understand the anticancer properties of the synthesized cocrystal. Treatments with concentrations of 7.5 and 10 μg/mL completely resisted the viability of A549 spheroids within day 01 and continued to have the same action without any relapse of the multicellular spheroid. At the same time, the cocrystal had no harmful effect on normal fibroblast cell spheroids (L929), indicating the drug's selectivity toward cancerous cells. Considering the overexpression of cannabinoid

https://doi.org/10.1021/acsomega.3c05617
ACS Omega 2023, 8, 46628−46639

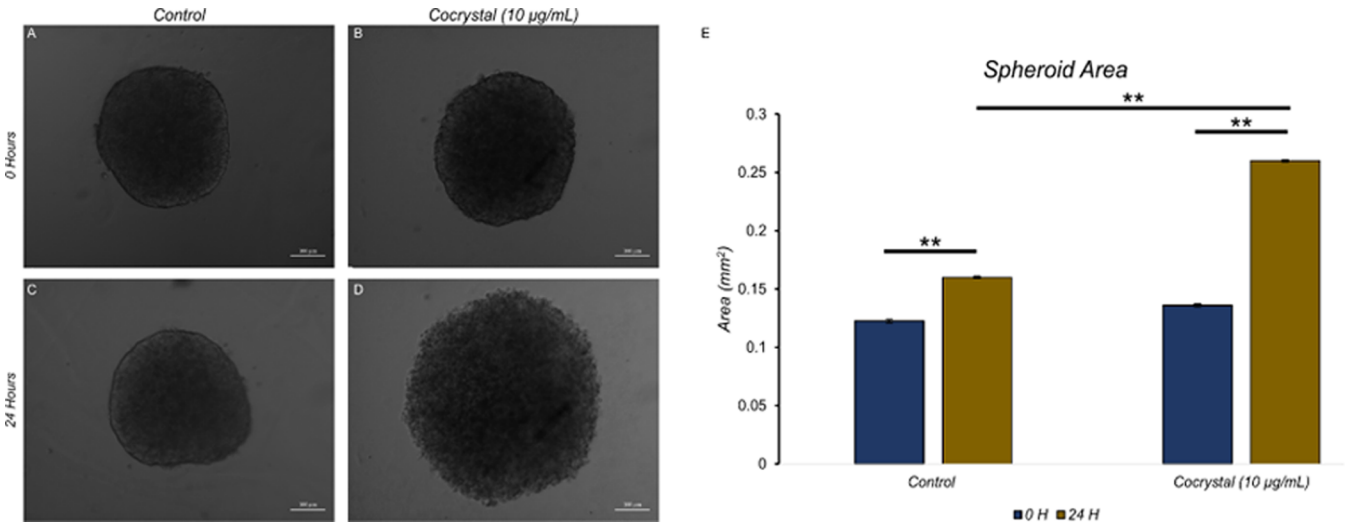

Figure 9. (A) Spheroid invasion assay: control A549 spheroids (a and d) at 0 and 48 h showing an increase in area with a significant number of invadopodia and A549 spheroid under cocrystal treatment. (B) Quantified surface areas of the control and cocrystal-treated spheroids.

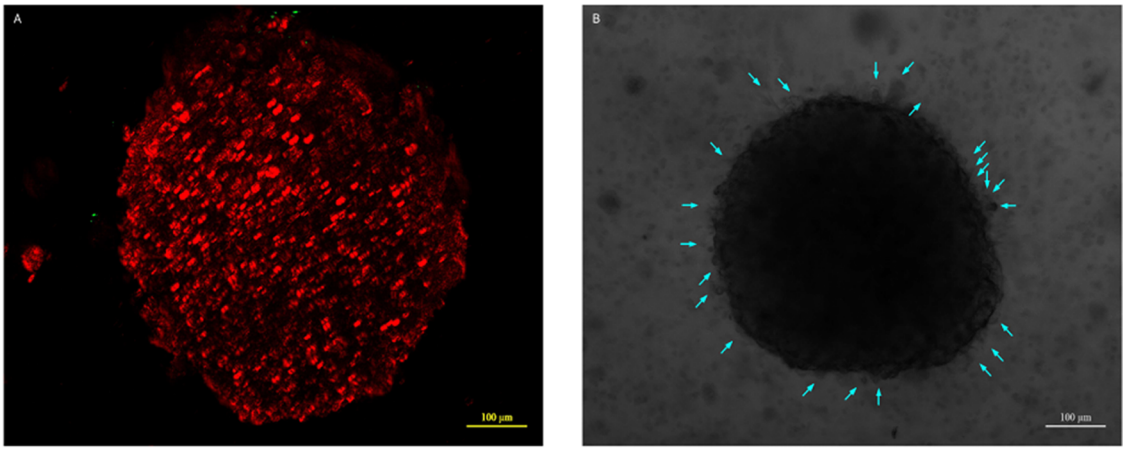

Figure 10. (A) Cocrystal (10 μg/mL)-treated spheroid completely died in 24 h and lost its integrity, observed with an increase in the surface area and (B) control spheroid (representative image) after 48 h showed multiple invadopodia formations (cyan arrows) from the periphery of the spheroid.

receptors in breast cancers, MCF7 spheroids were treated with the cocrystal (Figure S5), and the action remained the same. Multicellular spheroids used for the experiment mimic solid tumors *in vivo*, and the middle quiescent region of the spheroids is known to hold for multidrug resistance (MDR) during the treatment regime.[35] Drugs or small molecules can have severe consequences, killing not only the tumor cells but also the neighboring healthy tissues. Moreover, once the tumor microenvironment adapts to multidrug resistance (MDR), these drugs may become ineffective, leading to a loss in the fight against cancer. However, in the case of the cocrystal, the quinidine moiety overcomes MDR and related mechanisms by selectively sensitizing cancer cells with MDR to various other drugs. Previous reports demonstrate the selective features of quinidine, which can halt the proliferation of various cancers *in vitro*. Most lung cancers show overexpression of the epidermal growth factor receptor (EGFR), which is responsible for malignancies and an overall reduction in survival rates with a high risk of metastasis. At present, lung cancer remains a difficult disease to treat, with around 75% of cases remaining untreatable. Most lung cancers exhibit overexpression of EGFR, which is associated with malignancies, a decrease in survival rates, and a high risk of metastasis. Two oral anticancer drugs targeting EGFR have been approved for treating nonsmall cell lung cancer (NSCLC).[44,45] This is a significant development since lung cancer is a challenging disease to treat, and most cases show overexpression of EGFR, leading to malignancies and a reduction in survival rates with a high risk of metastasis.[46] In addition, Janus Kinase (JAK) I plays a significant role in the progression of mammary cancer along with its downstream STAT protein partners. Recent findings suggest that JAK receptors and proteins play a prominent role in hematological malignancies, accounting for about 50−95% of cases.[47] The low binding energy of the cocrystal with EGFR and JAK receptors and proteins makes it a promising candidate for targeting these receptors and proteins.

Spheroid Invasion Assay. To evaluate the ability of the MP−QU cocrystal to penetrate solid tumors, we treated spheroids of varying sizes and cell numbers ($0.8-1.6 \times 10^4$) with 10 μg/mL of the cocrystal and performed a live/dead assay after 24 h (Figure S6). The results demonstrated that the MP−QU cocrystal was effective in inhibiting cell proliferation regardless of spheroid size or cell number, indicating its high penetration efficiency *in vitro*. To further investigate this

https://doi.org/10.1021/acsomega.3c05617
ACS Omega 2023, 8, 46628−46639

efficiency, we tested the cocrystal on A549 spheroids embedded in matrigel at the same concentration. Treatment with the cocrystal led to a significant increase in the surface area of the spheroids (0.252 ± 0.01 mm^2) compared to control A549 spheroids (0.16 ± 0.001 mm^2) after 2 days (Figure 9a). To confirm that the spheroids were not viable, we differentially stained live and dead cells (FDA/PI) and observed their disintegration. In contrast, control A549 spheroids showed a high number of invadopodia formations protruding from the peripheral region, with 45 ± 2.516 (24 h) and 127 ± 2.516 (48 h) invadopodia formations. These results suggest that the MP−QU cocrystal can penetrate solid tumors effectively, inhibiting their growth without inducing invadopodia formations that could lead to metastasis.

Despite the observed selective anticell proliferative potential demonstrated by cell viability and live/dead assay (Figure 8), it is crucial for a drug molecule to have deep penetration into the central core of solid tumors. When the cocrystal was tested on spheroids of different sizes, consistent results were obtained, indicating its appreciable penetration efficiency (Figure S4). This property is important in overcoming multidrug resistance (MDR) and tumor reprogramming during treatment. Furthermore, some cancer cell populations progress from solid tumors to other tissues, resulting in metastasis. The cocrystal demonstrated interesting actions by inhibiting invadopodia formation from spheroids embedded in matrigel, which affect their viability within the first day of treatment. The Matrigel assay revealed that the treated spheroids lost their integrity and were not viable, while control spheroids exhibited multiple invadopodia (Figure 10b) formations from the periphery after 48 h. The cocrystal's penetration efficiency and invadopodia resistance can be attributed to its mechanism of action, which affects the viability of all regions of the spheroids, not just the periphery.[22,23] We present a cocrystal compound with promising potential in selectively inhibiting the proliferation of lung cancer cells. In a novel approach, we evaluated the efficacy of this pharmaceutical cocrystal using a 3D lung cancer model, which more closely resembles the architecture of solid tumors *in vivo* than traditional 2D models.[21−23] Our results demonstrate that the cocrystal not only exhibits potent anticancer properties but also demonstrates selectivity for cancerous cells over normal cells in this 3D cancer spheroid model.

CONCLUSIONS

Crystal engineering provides a versatile platform for post-synthetic functionalization of several important active pharmaceutical ingredients to enhance their physicochemical properties compared to their native drugs and find specific applications of interest. In this work, we successfully synthesized the pharmaceutical MP−QU cocrystal using the O−H···N heterosynthon. Importantly, there were no polymorphic changes in the grown cocrystals, as evidenced by the XRD pattern. DFT studies revealed the MP−QU interactions in different phases, leading to significant structural stability in terms of their bonding interactions and the corresponding changes in their electronic and optical characteristics. The MP−QU cocrystal has an enhanced selectivity toward cancerous and normal cells, which is demonstrated in 3D spheroids of highly metastatic nature (A549) and normal (L929) as well as breast cancer (MCF7) spheroids. The cocrystal also demonstrated resistance to the formation of invadopodia and migration in an invasion assay carried out under favorable environments. To recapitulate the real-time microenvironment features from genetic reprogramming to drug resistance, in vitro studies have been carried out in 3D spheroids that mimic *in vivo*-like solid tumors. At concentrations of 7.5 and 10 μg/mL, the MP−QU cocrystal was able to cease the proliferation of 3D spheroids within a day when compared to the control. Such swift action may not allow time for the cells to reprogram themselves for further resistance to the drug. Docking studies showed antimalarial and antibacterial properties of the synthesized cocrystal. Further studies at molecular levels and *in vivo* animal models are being conducted to decipher the overall pharmacological attributes of the cocrystal in our laboratory.

ASSOCIATED CONTENT

Supporting Information

The Supporting Information is available free of charge at https://pubs.acs.org/doi/10.1021/acsomega.3c05617.

Materials and methods; characterization; computational details; cell studies; culturing 3D spheroids; Alamar blue assay; Wst-01 cell viability assay; live/dead assay; spheroid invasion assay; powder X-ray diffraction; crystal data and structure refinement parameters; and docking studies (PDF)

AUTHOR INFORMATION

Corresponding Authors

Subha Narayan Rath − *Regenerative Medicine and Stem Cell Laboratory (RMS), Department of Biomedical Engineering, Indian Institute of Technology Hyderabad (IITH), Sangareddy, Telangana 502285, India*; Email: subharath@bme.iith.ac.in

Jai Prakash − *Department of Chemistry, Indian Institute of Technology (IIT) Hyderabad, Sangareddy, Telangana 502285, India*; orcid.org/0000-0002-4078-9662; Email: jaiprakash@chy.iith.ac.in

Authors

Sritharan Krishnamoorthi − *Department of Chemistry, Indian Institute of Technology (IIT) Hyderabad, Sangareddy, Telangana 502285, India*; orcid.org/0000-0003-4741-9100

Gokula Nathan Kasinathan − *Regenerative Medicine and Stem Cell Laboratory (RMS), Department of Biomedical Engineering, Indian Institute of Technology Hyderabad (IITH), Sangareddy, Telangana 502285, India*

Ganesan Paramasivam − *Department of Chemistry, Indian Institute of Technology (IIT) Madras, Chennai, Tamilnadu 600036, India*

Complete contact information is available at: https://pubs.acs.org/10.1021/acsomega.3c05617

Notes

The authors declare no competing financial interest.

ACKNOWLEDGMENTS

The authors acknowledge the Science and Engineering Research Board (SERB), Government of India, for financial support under a National Post-Doctoral Fellowship (N-PDF) Award (PDF/2017/000280/CS).

REFERENCES

(1) Zaworotko, M. J. Molecules to Crystals, Crystals to Molecules ... and Back Again? *Cryst. Growth Des.* **2007**, *7*, 4−9.
(2) Desiraju, G. R. Crystal and co-crystal. *CrystEngComm* **2003**, *5*, 466−467.
(3) Wuest, J. D. Co-crystals give light a tune-up. *Nat. Chem.* **2012**, *4*, 74−75.
(4) Zhu, W.; Zheng, R.; Fu, X.; Fu, H.; Shi, Q.; Zhen, Y.; Dong, H.; Hu, W. Revealing the Charge-Transfer Interactions in Self-Assembled Organic Cocrystals: Two-Dimensional Photonic Applications. *Angew. Chem., Int. Ed.* **2015**, *54*, 6785−6789.
(5) Bai, L.; Bose, P.; Gao, Q.; Li, Y.; Ganguly, R.; Zhao, Y. Halogen-Assisted Piezochromic Supramolecular Assemblies for Versatile Haptic Memory. *J. Am. Chem. Soc.* **2017**, *139*, 436−441.
(6) Sanphui, P.; Kumar, S. S.; Nangia, A. Pharmaceutical Cocrystals of Niclosamide. *Cryst. Growth Des.* **2012**, *12*, 4588−4599.
(7) Aakeröy, C. B.; Forbes, S.; Desper, J. Using Cocrystals to Systematically Modulate Aqueous Solubility and Melting Behavior of an Anticancer Drug. *J. Am. Chem. Soc.* **2009**, *131*, 17048−17049.
(8) André, V.; Fernandes, A.; Santos, P. P.; Duarte, M. T. On the Track of New Multicomponent Gabapentin Crystal Forms: Synthon Competition and pH Stability. *Cryst. Growth Des.* **2011**, *11*, 2325−2334.
(9) Springuel, G.; Leyssens, T. Innovative Chiral Resolution Using Enantiospecific Co-Crystallization in Solution. *Cryst. Growth Des.* **2012**, *12*, 3374−3378.
(10) Ghosh, S.; Bag, P. P.; Reddy, C. M. Co-Crystals of Sulfamethazine with Some Carboxylic Acids and Amides: Co-Former Assisted Tautomerism in an Active Pharmaceutical Ingredient and Hydrogen Bond Competition Study. *Cryst. Growth Des.* **2011**, *11*, 3489−3503.
(11) Chattoraj, S.; Shi, L.; Sun, C. C. Understanding the relationship between crystal structure, plasticity and compaction behaviour of theophylline, methyl gallate, and their 1: 1 co-crystal. *CrystEngComm* **2010**, *12*, 2466−2472.
(12) Gryl, M.; Seidler, T.; Stadnicka, K.; Matulková, I.; Němec, I.; Tesařová, N.; Němec, P. The crystal structure and optical properties of a pharmaceutical co-crystal- the case of the melamine-barbital addition compound. *CrystEngComm* **2014**, *16*, 5765−5768.
(13) Sekhon, B. S. Co-crystals of agrochemical actives. *Int. J. Agrochem. Plant Prot.* **2015**, *5*, 472−475.
(14) Saha, R.; Sengupta, S.; Kumar Dey, S.; Steele, I. M.; Bhattacharyya, A.; Biswas, S.; Kumar, S. A pharmaceutical cocrystal with potential anticancer activity. *RSC Adv.* **2014**, *4*, 49070−49078.
(15) Nicolov, M.; Ghiulai, R. M.; Voicu, M.; Mioc, M.; Duse, A. O.; Roman, R.; Ambrus, R.; Zupko, I.; Moaca, E. A.; Coricovac, D. E.; Farcas, C.; Racoviceanu, R. M.; Danciu, C.; Dehelean, C. A.; Soica, C. Cocrystal Formation of Betulinic Acid and Ascorbic Acid: Synthesis, Physico-Chemical Assessment, Antioxidant, and Antiproliferative Activity. *Front. Chem.* **2019**, *7*, 92.
(16) Zhang, Z.; Yu, N.; Xue, C.; Gao, S.; Deng, Z.; Li, M.; Liu, C.; Castellot, J.; Han, S. Potential Anti-Tumor Drug: Co-Crystal 5-Fluorouracil-nicotinamide. *ACS Omega* **2020**, *5* (26), 15777−15782.
(17) Usman, M.; Arjmand, F.; Khan, R. A.; Alsalme, A.; Ahmad, M.; Tabassum, S. Biological Evaluation of Dinuclear Copper Complex/Dichloroacetic Acid Cocrystal against Human Breast Cancer: Design, Synthesis, Characterization, DFT Studies and Cytotoxicity Assays. *RSC Adv.* **2017**, *7* (76), 47920−47932.
(18) George, C. P.; Thorat, S. H.; Shaligram, P. S.; Suresha, P. R.; Gonnade, R. G. Drug−drug cocrystals of anticancer drugs erlotinib−furosemide and gefitinib−mefenamic acid for alternative multi-drug treatment. *CrystEngComm* **2020**, *22* (37), 6137−6151.
(19) Khan, M.; Enkelmann, V.; Brunklaus, G. Crystal Engineering of Pharmaceutical Co-crystals: Application of Methyl Paraben as Molecular Hook. *J. Am. Chem. Soc.* **2010**, *132*, 5254−5263.
(20) McKim, J., Jr. Building a tiered approach to in vitro predictive toxicity screening: a focus on assays with in vivo relevance. *Comb. Chem. High Throughput Screening* **2010**, *13*, 188−206.
(21) Cox, M. C.; Reese, L. M.; Bickford, L. R.; Verbridge, S. S. Toward the Broad Adoption of 3D Tumor Models in the Cancer Drug Pipeline. *ACS Biomater. Sci. Eng.* **2015**, *1*, 877−894.
(22) Weiswald, L. B.; Bellet, D.; Dangles-Marie, V. Spherical Cancer Models in Tumor Biology. *Neoplasia* **2015**, *17*, 1−15.
(23) Rodrigues, T.; Kundu, B.; Silva-Correia, J.; Kundu, S. C.; Oliveira, J. M.; Reis, R. L.; Correlo, V. M. Emerging tumor spheroids technologies for 3D in vitro cancer modelling. *Pharmacol. Ther.* **2018**, *184*, 201−211.
(24) Abourahma, H.; Cocuzza, D. S.; Melendez, J.; Urban, J. M. Pyrazinamide cocrystals and the search for polymorphs. *CrystEngComm* **2011**, *13*, 6442−6450.
(25) Marder, S. R.; Perry, J. W.; Yakymyshyn, C. P. Organic Salts with Large Second-Order Optical Nonlinearities. *Chem. Mater.* **1994**, *6*, 1137−1147.
(26) Khan, M.; Enkelmann, V.; Brunklaus, G. Heterosynthon mediated tailored synthesis of pharmaceutical complexes: a solid-state NMR approach. *CrystEngComm* **2011**, *13*, 3213−3223.
(27) Sritharan, K.; Manikandan, V.; Srinivasan, K. A newer approach of growing methyl-p-hydroxybenzoate (p-MHB) single crystals from a melt without a polymorphic change in their form. *CrystEngComm* **2016**, *18*, 8237−8245.
(28) Bader, R. F. W. *Atoms in Molecules: A Quantum Theory*; Clarendon Press, 1994.
(29) (a) Popelier, P.; Popelier, P. L. A. *Atoms in Molecules: An Introduction*; Prentice Hall, 2000. (b) Gillespie, R. J.; Popelier, P. L. A. *Chemical Bonding and Molecular Geometry: From Lewis to Electron Densities*; Oxford University Press, 2001.
(30) Silvi, B. Chemical Bonding and Molecular Geometry: From Lewis to Electron Densities. *J. Mol. Struct.* **2002**, *610* (1−3), 277.
(31) Morris, G. M.; Goodsell, D. S.; Huey, R.; Olson, A. J. Distributed automated docking of flexible ligands to proteins: parallel applications of AutoDock 2.4. *J. Comput.-Aided Mol. Des.* **1996**, *10*, 293−304.
(32) DeLano, W. L. Pymol: An open-source molecular graphics tool. *CCP4 Newsl. Protein Crystallogr.* **2002**, *40*, 82−92.
(33) Takashi, T.; Iida, H.; Kitatani, Y.; Yokota, K.; Tsukagoshi, S.; Sakurai, Y. Effects of Quinidine and Related Compounds on Cytotoxicity and Cellular Accumulation of Vincristine and Adriamycin in Drugresistant Tumor Cells. *Cancer Res.* **1984**, *44*, 4303−4307.
(34) Wishart, G. C.; Bissett, D. L.; Paul, J.; Jodrell, D.; Harnett, A.; Habeshaw, T.; Kerr, D.; Macham, M. A.; Soukop, M.; Leonard, R. C. F. Quinidine as a resistance modulator of epirubicin in advanced breast cancer: mature results of a placebo-controlled randomized trial. *J. Clin. Oncol.* **1994**, *12*, 1771−1777.
(35) Preet, A.; Qamri, Z.; Nasser, M. W.; Prasad, A.; Shilo, K.; Zou, X.; Groopman, J. E.; Ganju, R. K. Cannabinoid Receptors, CB1 and CB2, as Novel Targets for Inhibition of Non-Small Cell Lung Cancer Growth and Metastasis. *Cancer Prev. Res.* **2011**, *4*, 65−75.
(36) Zhou, Q.; Zara, K. M.; Lucktong, A.; Moniwa, M.; Davie, J. R.; Strobl, J. S. Rapid induction of histone hyperacetylation and cellular differentiation in human breast tumor cell lines following degradation of histone deacetylase-1. *J. Biol. Chem.* **2000**, *275*, 35256−35263.
(37) Ru, Q.; Xiang, T.; Ming-shan, P.; Chen, L.; Yue, K. X.; Xiong, Q.; Bao-miao, M.; Li, C.-y. Voltage-gated K+ channel blocker quinidine inhibits proliferation and induces apoptosis by regulating expression of microRNAs in human glioma U87-MG cells. *Int. J. Oncol.* **2015**, *46*, 833−840.
(38) Pariante, C. M.; Kim, R. B.; Makoff, A. J.; Kerwin, R. W. Antidepressant fluoxetine enhances glucocorticoid receptor function in vitro by modulating membrane steroid transporters. *Br. J. Pharmacol.* **2003**, *139*, 1111−1118.
(39) Dhiman, N.; Shagaghi, N.; Bhave, M.; Sumer, H.; Kingshott, P.; Rath, S. Selective Cytotoxicity of a Novel Trp-Rich Peptide against Lung Tumor Spheroids Encapsulated inside a 3D Microfluidic Device. *Adv. Biosyst.* **2020**, *4*, No. e1900285.
(40) Wróbel, A. M.; Gregoraszczuk, EŁ. Actions of methyl-, propyl- and butylparaben on estrogen receptor-α and -β and the progesterone

https://doi.org/10.1021/acsomega.3c05617
ACS Omega 2023, 8, 46628−46639

receptor in MCF-7 cancer cells and non-cancerous MCF-10A cells. *Toxicol. Lett.* **2014**, *230*, 375−381.
(41) Lillo, M. A.; Nichols, C.; Perry, C.; Runke, S.; Krutilina, R.; Seagroves, T. N.; Miranda-Carboni, G. A.; Krum, S. A. Methylparaben stimulates tumor initiating cells in ER+ breast cancer models. *J. Appl. Toxicol.* **2017**, *37*, 417−425.
(42) Satoshi, Y.; Okamoto, Y.; Yamamoto, I.; Watanabe, K. Cannabidiol, a Major Phytocannabinoid, As a Potent Atypical Inhibitor for CYP2D6, Drug metabolism and disposition: the biological fate of chemicals. *Drug Metab. Dispos.* **2011**, *39*, 2049−2056.
(43) Padma, V. V. An overview of targeted cancer therapy. *BioMedicine* **2015**, *5*, 1−6.
(44) Sasaki, H.; Endo, K.; Okuda, K.; Kawano, O.; Kitahara, N.; Tanaka, H.; Matsumura, A.; Iuchi, K.; Takada, M.; Kawahara, M.; Kawaguchi, T.; Yukiue, H.; Yokoyama, T.; Yano, M.; Fujii, Y. Epidermal growth factor receptor gene amplification and gefitinib sensitivity in patients with recurrent lung cancer. *J. Cancer Res. Clin. Oncol.* **2008**, *134*, 569−577.
(45) Pao, W.; Miller, V.; Zakowski, M. F.; Doherty, J.; Politi, K.; Sarkaria, I. EGF receptor gene mutations are common in lung cancers from "never smokers" and are associated with sensitivity of tumors to gefitinib and erlotinib. *Proc. Natl. Acad. Sci. U.S.A.* **2004**, *101*, 13306−133011.
(46) Wehde, B. L.; Rädler, P. D.; Shrestha, H.; Johnson, S. J.; Triplett, A. A.; Wagner, K. U. Janus Kinase 1 Plays a Critical Role in Mammary Cancer Progression. *Cell Rep.* **2018**, *25*, 2192−2207.
(47) Thomas, S. J.; Snowden, J.; Zeidler, M.; Danson, S. J. The role of JAK/STAT signalling in the pathogenesis, prognosis and treatment of solid tumours. *Br. J. Cancer* **2015**, *113*, 365−371.

NOTE ADDED AFTER ASAP PUBLICATION

This paper was originally published ASAP on November 21, 2023. The TOC graphic was replaced, and the paper reposted on November 27, 2023.

https://doi.org/10.1021/acsomega.3c05617
ACS Omega 2023, 8, 46628−46639